
EXPLAINABLE MACHINE-LEARNING BASED DETECTION OF KNEE INJURIES IN RUNNERS

A PREPRINT

David Fuentes-Jiménez^{*1}, Sara García-de-Villa^{†2}, David Casillas-Pérez^{‡2}, Pablo Floría^{§3}, and Francisco-Manuel Melgarejo-Meseguer^{¶2}

¹Department of Electronics, University of Alcalá, Alcalá de Henares, 28801, Spain

²Department of Signal Processing, Universidad Rey Juan Carlos, Fuenlabrada, 28942, Spain

³Physical Performance & Sports Research Center (CIRFD), Universidad Pablo Olavide, Sevilla, 41013, Spain

February 13, 2026

ABSTRACT

Running is a widely practiced recreational activity, yet it is associated with a high incidence of knee injuries, particularly Patellofemoral Pain Syndrome (PFPS) and Iliotibial Band Syndrome (ITBS). Accurate patterns associated with these injuries has the potential to impact clinical decision-making. Achieving this requires precise systems capable of capturing and analyzing the temporal kinematic data of human motion. In this study, optical motion capture systems are employed to improve the detection of injury-related gait patterns. A publicly available dataset comprising 839 treadmill motion recordings from both healthy and injured runners is analyzed to assess the effectiveness of these measurement systems in capturing dynamic movement parameters relevant to injury classification. Our study focuses on the stance phase of the running gait, examining time series of joint and segment angles derived from motion capture data, alongside discrete point values. We evaluate three classification scenarios: (1) healthy vs. injured runners, (2) healthy vs. PFPS, and (3) healthy vs. ITBS. We explore various feature input spaces, ranging from traditional point-based metrics to full time series representations of the stance phase, as well as hybrid approaches combining both. Multiple classification models are employed, including classical algorithms such as K-Nearest Neighbors, Gaussian Processes, and Decision Trees, as well as deep learning architectures like Convolutional Neural Networks (CNNs) and Long Short-Term Memory networks (LSTMs). Model performance is assessed using accuracy, precision, recall, and F1-score metrics. Additionally, we incorporate explainability techniques such as Shapley values, Partial Dependence Plots, saliency maps, and Grad-CAM to interpret model decisions. Our results demonstrate that combining time series data with point values significantly enhances detection performance. Deep learning models outperform classical approaches, with CNNs achieving the highest accuracy: 77.9% for PFPS, 73.8% for ITBS, and 71.43% for the combined injury class (PFPS+ITBS). These findings underscore the effectiveness of motion capture systems with advanced machine learning techniques in identifying knee injury-related running patterns.

Funding: This study was partially supported by the Spanish Ministry of Science, Innovation and Universities (MICIU/AEI/10.13039/501100011033), HERMES project (Grant No. PID2023-152331OA-I00), METAMORPH project (Grant No. PID2023-151295OB-I00) and LATENTIA project (Grant No. PID2022-140786NB-C31) and by the Community of Madrid with the Industrial Doctorates CAM 2024 project (IND2024/TIC-33917).

^{*}d.fuentes@uah.es

[†]sara.garcia.devilla@urjc.es

[‡]david.casillas@urjc.es

[§]pfloriam@upo.es

[¶]francisco.melgarejo@urjc.es

Keywords motion analysis · running patterns · patellofemoral · iliotibial band · Machine Learning

1 Introduction

Running is one of the most popular recreational physical activities. However, it is associated with a high incidence rate of musculoskeletal injuries, ranging from 4 to 33 per 1 000 hours of running Videbaek et al. [2015]. Among recreational runners, the knee is the most frequently affected joint, with iliotibial band syndrome (ITBS) and patellofemoral pain syndrome (PFPS) being the most common diagnoses Taunton et al. [2002]. The causes of these injuries are multifactorial, involving complex interactions between external variables (e.g., training load, volume) and internal factors (e.g., biomechanics, age) Van der Worp et al. [2015].

The identification of movement patterns associated with health conditions enables the development of prognostic indices that support injury prevention and long-term health maintenance with gait interventions Crowell and Davis [2011], Soltanabadi et al. [2023], Keast et al. [2022]. In the context of runners, detecting such patterns requires accurate quantification of motion during running, followed by uni- or multi-parametric analysis and data analysis algorithms.

Previous research demonstrate the potential of gait pattern analysis for predicting adverse health outcomes, such as neurodegenerative diseases Cicirelli et al. [2021a], Hammoud et al. [2025], Shcherbak et al. [2023] or injury risk Lee et al. [2022], Zeng et al. [2020], Kokkotis et al. [2022], using both camera-based systems and wearable sensor technologies. These findings highlight the value of motion analysis in clinical and preventive applications.

Despite the advances in gait analysis, the study of injury-related movement patterns in running remains an emerging research area. Several investigations have aimed to identify similar kinematic gait patterns among runners with injuries using optical motion capture systems Zhuang et al. [2025], but current evidence is insufficient to create meaningful running-related risk profiles Ceyssens et al. [2019]. This lack of agreement can arise from the limited sample sizes, the loss of information in the reduction of time series of data to biomechanical point values, such as peak values Phinyomark et al. [2017], or the study of running-related injuries in general Willwacher et al. [2022], misrepresenting the significance of a particular biomechanical risk factor for specific injuries Ceyssens et al. [2019].

Pattern recognition techniques, such as clustering algorithms, are applied to classify runners and uncover biomechanical patterns related to injury risk Dingenen et al. [2020], Jauhainen et al. [2020], Martin et al. [2022], Senevirathna et al. [2023]. However, the results indicate that while subgroups with homogeneous movement patterns can be identified, a direct association with injury risk is not evident. To the best of our knowledge, only one supervised Machine Learning (ML) method is applied for injury risk detection Eskofier et al. [2012], specifically to identify PFPS. Consequently, alternative supervised ML methods are not being explored for this analysis. One possible reason for this lack of use is the black-box behavior of ML methods, which limit their use for clinical applications. However, recent advances in explainability algorithms make it possible to unravel the model predictions in relation with their inputs.

This work aims to investigate the effectiveness of joint angle time series and kinetic descriptors from optical motion capture systems in distinguishing knee-injured runners from healthy ones; assessing the performance of supervised ML methods. The ML methods analyzed include both classical and modern algorithms, such as Deep Learning (DL) models. Additionally, we enhance the explainability of our results by applying explainability algorithms to unravel the black-box behavior of the applied methods.

This paper extends the work presented in the proceedings paper in Fuentes-Jiménez et al. [2025], by expanding the DL algorithms analyzed and enhancing the methods' explainability. The study now includes both Convolutional Neural Networks (CNNs) and Long Short-Term Memory networks (LSTMs), in addition to the classical ML models. The classification metrics for all algorithms are provided, along with a detailed account of hyperparameter optimization. Furthermore, the explainability analysis has been increased by incorporating four new methods, resulting in more insightful findings for the best-performing algorithms.

The remainder of this manuscript is structured as follows: Section 2 reviews previous work on injury pattern identification using kinematic information; Section 3 describes the database of runners utilized in this study, the methodology applied, including the algorithms used, their implementation, and the metrics for their analysis, and the explainability methods; Section 4 presents the classification metrics of the classifiers under analysis and the results of the explainability analysis, with an in-depth examination of the features, followed by the discussion of these results; finally, Section 5 provides the conclusive remarks on the detection of injury patterns using supervised algorithms and the feature analysis based on the explainability.

2 State of the art

The study of the temporal dynamics of movement has been widely investigated in relation to gait, specially for detecting neurological diseases Kokkotis et al. [2022], Cicirelli et al. [2021b]. For instance, in Xia and Cao [2026], Raja et al. [2026] human motion dynamic is extracted from video records and wearable sensors, and then processed by a graph convolutional network to detect freezing of gait in Parkinson's disease patients. In Ru et al. [2025] a gait analysis is used to classify among Parkinson's disease, amyotrophic lateral sclerosis, and Huntington's disease using machine learning methods.

With respect to motion-related injuries, in Moura et al. [2025], gait kinematic is used for detecting knee osteoarthritis prediction by deep learning methods. In García-de-Villa et al. [2024], kinematic and spatio-temporal gait parameters from inertial analysis are used for assessment of fall risk.

In sports science, there are fewer studies that have employed dynamic motion analysis to minimise injury risk and enhance athletic performance. In Liu et al. [2025], a 1D-CNN is trained to classify swimming patterns during the training to improve efficiency. In Chen and Jia [2025], complex dynamic patterns during the tennis strokes are detected and classified to the enhance motion efficiency and to prevent sports injuries using kinetic chain theory analysis.

Focusing on running injuries, the work Eskofier et al. [2012] is one of the first studies to select generic biomedical features for classifying gender, shod/barefoot, and injury pattern groups, specifically focusing on PFPS vs non-injured runners. It uses AdaBoost for the classifications, tested using leave-one-subject-out cross validation. The study achieves perfect identification of PFPS based on the hip abduction moment, after matching mileage, experience, and weight among non-injured and injured individuals. These results are promising for identifying differences between PFPS and non-injured running patterns. However, the findings are limited to six injured volunteers, and further analyses of larger databases have not been able to determine a simple identification of the PFPS pattern.

More recently, authors in Dingenen et al. [2020] develop a larger analysis with 53 recreational runners, with running-related injuries. The study evaluates the foot and tibia inclination at initial contact, and hip adduction and knee flexion at mid-stance in both frontal and sagittal planes, which are tracked by video marker analysis during shod running on a treadmill at preferred speed. The four outcome measures were clustered using K-means cluster analysis where the silhouette method were conducted to detect optimal number of clusters. This study does not establish any pattern for the injuries: the same injury can be represented with more than one kinematic representation and one pattern can be related to different injuries.

The study in Jauhainen et al. [2020] identifies distinct subgroups with homogeneous running patterns among a large group of injured and non-injured runners, 291 injured and non-injured runners representing both sexes and a wide range of ages (10 – 66 years). Clusters are calculated using a hierarchical clustering method through kinematic data provided by a motion capture over categories of injuries according to the body location (knee, ankle/foot, and hip/pelvis) The results prove that runners with the same injury types do not group together.

Hierarchical clustering is also used to detect different clusters in a 134 injured and uninjured runner database, based on their kinetic gait patterns Senevirathna et al. [2023]. The gait patterns are analyzed based on gait parameters commonly associated with running injuries, such as the contact time, average loading rate or vertical impulse force. The results reveal clusters of runners, but none association with the injury status.

Hierarchical clustering is also applied for specific injuries, as in Martin et al. [2022], where it is utilized for identifying bone stress injury (BSI) risk. This study analyzes a 53 collegiate runners database using pelvis and femur geometry from *Dual-energy X-ray Absorptiometry* (DXA) scans. The geometry is reduced by a principal components analysis for the study. The results provide seven distinct groups revealing differences between groups in pelvis and proximal femur geometry related to the lower body BSI incidence during the subsequent academic year.

Previous works are aimed at finding injury-related patterns mainly focus on unsupervised methods that mainly evaluate punctual kinematic descriptors, such as velocity, as point values. Most of them group runners using the hierarchical clustering method Jauhainen et al. [2020], Martin et al. [2022], Senevirathna et al. [2023]. None of the reviewed studies perform a comparison of supervised or unsupervised methods to verify whether the resulting clusters are consistent. Except for Eskofier et al. [2012], no supervised methods are applied for the classification task, mainly due to the difficulty of identifying the most relevant features; moreover, none of them rely on recent deep neural network (DNN) models. This paper aims precisely to provide a deeper analysis of more supervised classification techniques in the identification of running injury risk with a focus on their explainability.

With the exception of Martin et al. [2022], which uses parameters derived from DXA scans, most studies rely only on point-based features such as speed, joint inclination, temporal values at specific instants, or contact time, without incorporating the full dynamics as model inputs. The databases employed are generally small, which limits their

representativeness of groups of runners with different types of injuries. In most cases, the analyzed injury type is generic in location, with the exception of Eskofier et al. [2012] which focuses on PFPS. This heterogeneity in running patterns highlights the need to particularize the analysis by injury type in order to identify more specific movement patterns that allow for better discrimination.

The work Fuentes-Jiménez et al. [2025] is the first to provide a comparison of supervised ML methods, including a recent DNN-based method, for detecting knee injuries, and it includes a saliency map for explainability analysis. However, this study does not explore alternatives that exploit temporal dependencies, such as LSTMs, and the explainability analysis is limited to the application of a single method on the CNN, which the present study surpasses. In light of these limitations of the state of the art, in this study, we propose a supervised-based framework that includes the analysis of complete stance phase time series combined with kinematic descriptors. The key contributions of this study are as follows: *a*) analysis of classical ML methods in ITBS and PFPS patterns identification using time series and kinematics descriptors, providing the details regarding the hyperparameters optimization, *b*) improvement of the novel DL proposal, especially using time series, including CNNs and LSTMs, and *c*) unraveling the black-box behavior to bring understandability to the methods that yield the highest classification metrics in the injury pattern identification by applying five novel explainability-based algorithms.

3 Materials and Methods

3.1 Running database

We focus on the recently published database Ferber et al. [2024] of non-injured and injured runners during treadmill running. Briefly, the database is composed of 1 798 runners with different injury status and includes treadmill running motion records, which are measured through high-speed optoelectronic infrared motion capture cameras (Vicon, Oxford, UK).

Our study focuses on the analysis of two common knee injuries: the PFPS and ITBS. The database Ferber et al. [2024] includes 137 and 100 runners with PFPS and ITBS, respectively, and 396 non-injured runners. Some runners have several records, so after assigning one sample per record, we analyze 137, and 126 records from runners with PFPS and ITBS, respectively and 576 from non-injured runners.

Each recording sample includes socio-demographic and anthropometric variables and *time series* raw marker trajectories. The variables describe the volunteers' age, dominant leg, gender, height, weight, and running-related injuries. Marker trajectories describe the motion of seven anatomical structures: the two feet, two shanks, two thighs, and the pelvis.

3.2 Data preprocessing

We use the codes in the database supplemental materials Ferber et al. [2024] in the data preprocessing, whose flowchart is depicted in Fig. 1. We calculate the X-Y-Z Cardan angles from six joints: ankles, knees, hips, and three segments: feet and the pelvis. For the left foot stance, the angles of the left ankle, knee, hip and foot, and pelvis are segmented. Similarly, for the right foot stance, the angles of the right ankle, knee, hip and foot, and pelvis are segmented. We also extract the running point values. Using the feet angles with respect to the global frame, we segment the time series into running steps using principal component analysis to detect touch-down and toe-off events on the basis of Osis et al. [2014]. Our analysis is limited to the running stance phase, between each touch-down and toe-off events. Since steps may have different number of samples, we use cubic interpolation to equalize the number of samples to 101 samples. The *time series* used in this study are the mean angles and the upper-and lower-envelope angles during the stance phase of the segmented strides.

3.3 Kinematic, spatio-temporal and power parameters

From the normalized angle time series, we derive the following running spatio-temporal parameters: step width, stride rate and length, % swing and stance times, pelvis drop angle and excursion, % time with ankle in eversion, ankle dorsiflexion angle peak, and eversion and rotation angles peak and excursion, knee flexion angle peak, and adduction abduction and rotation angles peak and excursion, hip extension angle peak, and adduction and rotation angles peak and excursion, foot progression angle, medial heel whip excursion in take off, pronation onset and offset, velocity peaks of ankle eversion and rotation, knee abduction, adduction and rotation, hip adduction, abduction and rotation, pelvic drop and vertical oscillation, which are added to the register descriptive variables to form the set of *point values*. We also include the power of the rotation time series for each angle in the 0-1 Hz, named LF, 1-3 Hz, named MF, and 3-99 Hz, named HF, frequency bands, with the aim of capturing differences about running speeds.

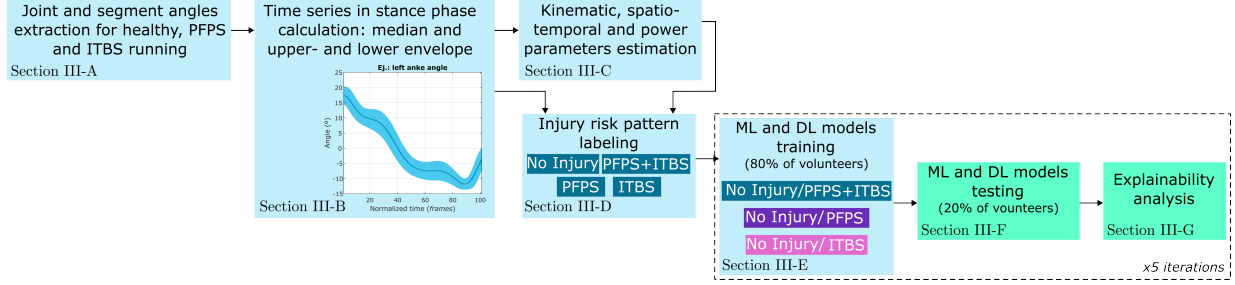


Figure 1: Methodology flowchart from the joint and segment angles in the database, including the time series in the stance phase extraction and running spatio-temporal parameters calculation, until the injury pattern identification with the ML and DL models, along with their explainability analysis.

3.4 Injury risk identification

We study three different binary classifications: we detect knee-injured vs. non-injured runners, considering PFPS and ITBS gathered as a single injured class; then, we focus on detecting runners with PFPS against non-injured runners; and finally, we exclusively detect runners with ITBS versus non-injured runners.

We analyze our hypothesis that time series include more relevant information for injury risk pattern detection than point values by evaluating the models' performance with different sets of inputs. Firstly, we evaluate the injury pattern identification when classifiers only receive the time series. Secondly, we study the influence of point values added to the time series. Lastly, in order to have a baseline scenario, we assess the classifiers with only point values as inputs.

3.5 Machine learning classifiers

The classifiers evaluated for the injury risk identification task are 8 supervised ML algorithms and 2 DL-based methods. The classifiers evaluated are described below, along with the hyperparameters chosen through grid search optimization.

K-Nearest Neighbors (KNN) Shakhnarovich et al. [2008], James et al. [2013] is a non-parametric supervised algorithm. KNN identifies the k closest training examples to a query point in the feature space and assigns the most common class label, i.e. the running pattern class label, among these neighbors. It relies on a distance metric to determine proximity and on k , which is optimized with a grid search between 2 and 12, and a step equal to 1.

Support Vector Machine (SVM) Schölkopf et al. [2002], James et al. [2013] is a robust supervised learning algorithm. SVMs find the optimal hyperplane that maximizes the margin between different running pattern classes in the feature space. This hyperplane is determined by the support vectors, which are the data points closest to the decision boundary. Its kernel function allows SVMs to operate in a higher-dimensional space without explicitly transforming the data. In this article, we use two kernels, linear (SVM_L) and a polynomial (SVM_P). The regularization parameter of the SVM_L is optimized with grid search within the values 0.0001, 0.001, 0.005, 0.01, 0.02, 0.03, 0.04, 0.05 and 0.06. For the SVM_P , the regularization parameter is optimized with grid search between 0.1 and 1.1 with a step of 0.1, and all the degrees from 2 to 5 were analyzed.

Gaussian Processes (GPs) Rasmussen [2003] are non-parametric and probabilistic ML models. GPs represent a continuous random process of a dense variable. GP models predict the running pattern class by introducing a set of latent variables from a Gaussian process.

Decision Trees (DTs) Rokach and Maimon [2005], James et al. [2013] are graph-based supervised ML models. A DT constructs a decision process by recursively splitting the feature space into distinct and non-overlapping regions. DTs predict the running pattern class by partitioning the feature space based on the values of the input variables. We optimize the maximum depth, evaluating the case without maximum or maximum depth equal to 5, 10, 20 and 30. The assessed values for the sample division per node are 2, 5 and 10, and 1, 2 and 4 minimum samples per leaf. Both Gini criteria are analyzed for optimization and for the splitter parameter, the most informative split criterion and the random ones are evaluated, with the options of `sqrt` and `log2` for controlling the number of features.

Adaptive Boosting (ADB) Ferreira and Figueiredo [2012], González et al. [2020] is a boosting ensemble ML method. It works by sequentially combining multiple weak learners to create a strong classifier. The algorithm iteratively adjusts the weights of the training samples, focusing more on those that were misclassified by previous learners. Each weak learner is trained on a weighted version of the dataset, and the final model provides the weighted vote of the

running pattern class estimated by these weak learners. We use DTs as weak learners, with the optimization of the hyperparameters described for DTs, except for the number of estimators.

Random Forests (RFs) Breiman [2001], James et al. [2013] are an ensemble ML method that combines the output of multiple DTs to overcome their overfitting tendency. RFs create sets of independent DTs using a random subset of the data and features during the training. The output of the RF is the pattern label selected by most trees. We optimize the estimator number between 100 and 300, maximum depth between 10 and 20, minimum samples per split between 2 and 10, minimum samples per leaf between 1 and 4. Three partitioning criteria were evaluated, being the Gini impurity and two metrics based on Shannon’s information theory: entropy and logistic loss.

Artificial Neural Networks (ANNs) Bishop et al. [1995], James et al. [2013] are ML models inspired by the structure and function of biological neural networks in the human brain. They consist of interconnected artificial neurons organized into layers. ANNs predict the running pattern class by passing the input variables through multiple layers of neurons. Each neuron processes the input using a weighted sum and an activation function, which introduces non-linearity into the model. Our activation function is ReLu, with 1 layer and we optimize the number of neurons between 1 and 100 and the maximum iterations between 100 and 1000.

Convolutional Neural Networks (CNNs) LeCun et al. [2015], are a type of Deep Neural Network (DNN) that uses a series of convolutional layers to extract intrinsic features, named deep features, from the input data, which enable CNNs to excel in classification tasks.

The CNN architecture for the time series is as follows: The input consist of 2 separated input branches. a) The main one that consist of joint-temporal data with shape (T, A, C) , where T is the number of time steps, A the number of articulations, and C the number of channels. b) The secondary one that uses sparse features processed in parallel. After passing through input a) of the neural network, the next layer consist of a Gaussian noise layer with a standard deviation of 0.05, used for regularization. Once regularized, we perform feature extraction using two consecutive Inception-based residual blocks Szegedy et al. [2017] with 64 filters each one. These feature extraction allow a multiscale processing preserving the information through the residual connections. We use after the feature extraction Squeeze-and-Excitation (SE) Hu et al. [2018] modules to emphasize the most useful feature channels suppressing spurious responses. We use a Dropout with a rate of 0.3 after the first block to reduce overfitting. Once we pass all these layers, the resulting maps are flattened to obtain a fixed-length representation of the input time series.

Starting from the secondary branch, where we have the sparse features, they are processed in parallel with respect to the first part of the network. The second branch consist of a dense layer with 8 neurons and L2 regularization, followed by batch normalization, SiLU activation, and dropout with a rate of 0.3. A second dense layer with 16 neurons is then applied, followed by batch normalization and SiLU activation. These secondary outputs are then concatenated with the flattened maps obtained from the first representation of the input time series.

Finally the fused features are followed by a dense layer with 16 neurons and L2 regularization, followed by batch normalization and SiLU activation. The last layer of the network is composed by a dense layer with a sigmoid activation that performs the binary classification.

The training was carried out using RMSprop optimizer with a learning rate of 10^{-4} , $\rho = 0.9$, and gradient accumulation over 2 steps. We used as loss the binary crossentropy and we evaluated as metrics during the training the accuracy, precision and recall. Additionally we used data generators in training that mitigate class-imbalance effects.

Long Short-Term Memory (LSTM) Hochreiter and Schmidhuber [1997] is a specialized recurrent neural network (RNN) architecture designed to model long-range dependencies in sequential data while mitigating the vanishing gradient problem inherent in traditional RNNs. It achieves this through a memory cell that maintains state over time, regulated by three gating mechanisms: the input gate, which controls the flow of new information into the cell; the forget gate, which determines the extent to which previous cell states are retained or discarded; and the output gate, which governs the exposure of the internal state to the next layer or time step. These gates are implemented using sigmoid activations and element-wise multiplications, enabling fine-grained control over information propagation and retention. This structure allows LSTMs to effectively learn temporal patterns in complex sequences such as financial time series, natural language, or physiological signals.

In this work we propose to use multivariate temporal data structured as temporal sequences for each joint. The network input consist of a tensor with a fixed length of 101 time steps, 10 articulations, and 9 channels corresponding to Roll, Pitch, and Yaw coordinates each one of three different post processed modalities.

The proposed recurrent neural network in this work is based on LSTM recurrent structures and begin with a bidirectional one-dimensional convolutional LSTM layer with 30 filters and a kernel size of 3, which enables the joint modeling of spatial correlations across articulations and temporal dynamics across time. We return the processed sequences in order to preserve temporal resolution for subsequent processing and apply a recurrent dropout with a coefficient of 0.4. Once

we pass this layer, we collapse using a flattening the spatial dimensions of each time step into a single feature vector. These collapsed features are used to feed another bidirectional LSTM layer with 20 neuronal units and a dropout rate of 0.2. In this case we don't return the sequences, obtaining a single output that represents the latent space and their associated input temporal sequence. Finally the latent representation is processed by a fully connected layer with 10 neurons and ReLU activation, followed by a last dense output layer with a single neuron and sigmoid activation.

The training was carried out using RMSprop optimizer with a learning rate of 10^{-4} , $\rho = 0.9$, and gradient accumulation over 2 steps. We used as loss the binary cross entropy and we evaluated as metrics during the training the accuracy, precision and recall. Additionally we used data generators in training that mitigate class-imbalance effects.

3.6 Classification metrics for injury risk detection

We evaluate the models' performance in the running pattern classification with four classification metrics: accuracy (ACC), precision (PRE), recall (REC) and F1-score ($F1$):

$$ACC(\%) = \frac{TP + TN}{P + N} \cdot 100 \quad (1)$$

$$PRE(\%) = \frac{TP}{TP + FP} \cdot 100 \quad (2)$$

$$REC(\%) = \frac{TP}{TP + FN} \cdot 100 \quad (3)$$

$$F1(\%) = \frac{2 \cdot TP}{2 \cdot TP + FP + FN} \cdot 100 \quad (4)$$

where TP , TN , FP , FN , P and N are the true positives, true negatives, false positive, false negative, positive and negative labels. In this paper, negative labels always correspond to healthy running pattern class, and positive labels refer to the injury running pattern class, which is PFPS+ITBS, PFPS or ITBS, depending on the classification problem.

The analyzed classifiers are evaluated using 5-fold cross-validation on the volunteers to ensure that those in the test set are not included in the training set. Iteratively, we use the time series and point values of 80% of volunteers to train the classifiers and the information of the remaining 20% for testing. The classification metrics provided correspond to the averaged metrics for all test sets with their standard deviation.

3.7 Explainability

In this work, we employ several methods to enhance the explainability of our models and assist clinicians in better understanding the relationships between different types of movements and injuries. These methods range from feature-based approaches—such as Shapley values to model-based techniques like Saliency Maps and Grad-CAM.

Shapley values Štrumbelj and Kononenko [2013] serve to quantify the contribution of each feature to the model prediction by considering all possible combinations of features. From a mathematical perspective, the Shapley value of a feature is defined as the average marginal contribution of that feature across all possible subsets of features. This approach is grounded in cooperative game theory, where each feature is treated as a “player” in a game whose “payout” is the model’s output. The result is a fair and consistent allocation of importance scores, reflecting how much each feature contributes to the prediction in different contexts.

Saliency maps enhance explainability in complex systems like DNNs by identifying and visualizing input areas that significantly influence model decisions. They are generated by calculating output derivatives with respect to each input feature, highlighting regions with the greatest effect on predictions Simonyan et al. [2013]. In this way, regions with greater effects in the output prediction for an associated class are highlighted.

Grad-CAM Selvaraju et al. [2017] is a visualization technique that helps us understand which parts of the input signal are most influential in the model’s final decision. This method is primarily designed for CNNs and is based on a weighted combination of the gradients of the output with respect to the activation maps from a convolutional layer, typically just before the softmax layer. The output is a heatmap that highlights the regions of the input that contribute most strongly to the model prediction.

Saliency maps and Grad-CAM are very useful in inputs whose visualization is intuitive for human perception, generally images, but they are portable to other cases, such as the one addressed here, representing the information used as 2D maps to give clues for the detection of injury patterns. We represent the cumulative influence of each of the angle time series with heat maps, in order to analyze their influence for detecting PFPS and ITBS.

Table 1: Detection accuracy for PFPS+ITBS, PFPS and ITBS gathered according to the input parameters in classifiers. Accuracy is provided in %. The two highest accuracy metrics for each input set and injury pattern detection are highlighted in bold letters.

Model	Time series			Time series & Point values			Point values		
	PFPS+ITBS	PFPS	ITBS	PFPS+ITBS	PFPS	ITBS	PFPS+ITBS	PFPS	ITBS
KNN	55.8 \pm 2.0	62.4 \pm 3.0	60.0 \pm 6.5	57.6 \pm 4.5	64.6 \pm 3.3	59.4 \pm 4.2	61.2 \pm 4.8	67.3 \pm 5.4	62.5 \pm 6.8
SVM _L	62.2 \pm 4.8	71.5 \pm 5.3	61.1 \pm 7.6	63.4 \pm 3.4	71.7 \pm 4.2	60.5 \pm 9.5	58.0 \pm 7.4	67.4 \pm 4.3	56.8 \pm 7.5
SVM _P	58.3 \pm 8.2	64.9 \pm 4.6	55.0 \pm 3.1	60.3 \pm 7.9	63.7 \pm 3.0	54.1 \pm 4.2	56.7 \pm 8.0	62.8 \pm 4.7	56.1 \pm 6.1
GP	63.7 \pm 5.5	61.1 \pm 10.2	63.5 \pm 10.8	66.0 \pm 3.8	65.3 \pm 8.0	60.1 \pm 7.1	62.8 \pm 6.3	69.5 \pm 3.7	62.5 \pm 5.3
DT	53.7 \pm 7.5	55.8 \pm 8.7	53.5 \pm 8.2	54.5 \pm 5.3	51.6 \pm 7.5	56.0 \pm 7.5	49.7 \pm 2.8	56.4 \pm 4.3	51.0 \pm 5.3
ADB	60.9 \pm 6.1	67.6 \pm 7.1	56.5 \pm 6.9	58.8 \pm 5.2	64.9 \pm 5.9	58.9 \pm 13.9	60.6 \pm 8.0	62.3 \pm 6.3	61.6 \pm 8.3
RF	61.5 \pm 3.2	65.3 \pm 2.1	63.6 \pm 8.3	60.4 \pm 9.1	67.2 \pm 4.7	61.4 \pm 7.3	60.0 \pm 6.5	65.5 \pm 4.7	61.7 \pm 5.8
ANN	58.0 \pm 2.9	67.5 \pm 4.0	61.1 \pm 10.7	58.4 \pm 4.4	72.1 \pm 7.2	59.6 \pm 8.4	60.5 \pm 6.9	69.7 \pm 7.0	65.3 \pm 10.2
CNN	71.4 \pm 1.8	76.2 \pm 1.8	73.8 \pm 2.0	70.5 \pm 1.7	77.9 \pm 1.2	73.3 \pm 1.6	—	—	—
LSTM	65.1 \pm 1.5	71.5 \pm 1.6	66.7 \pm 2.5	—	—	—	—	—	—

In our approach, these explainability techniques are applied to the ML and DL models that achieve the best performance. Specifically, we provide the results as the average response across positive cases from one of the test set folds. Saliency Maps and Grad-CAM, although originally designed for image data, were adapted to our context by representing the input time series as 2D maps. This allows us to highlight the temporal regions and joint angles that most influenced the model’s predictions. The resulting heatmaps provide valuable insights into the biomechanical patterns associated with PFPS and ITBS, offering clinicians interpretable visual cues that may support injury diagnosis and prevention strategies.

4 Results and discussion

4.1 Optimized hyperparameters

The optimal hyperparameters for each classification model were determined through grid search. For the KNN algorithm, the best performance was achieved using the Euclidean distance metric and $k = 7$. The SVM_L yielded optimal results with a regularization parameter of 0.001, while SVM_P performed best with a regularization parameter of 1.1 and a polynomial degree of 3. The DT model was optimized with a maximum depth of 10, maximum features set to sqrt, a minimum of 2 sample per leaf, and 2 samples per split, using a random splitting strategy. For the RF classifier, the best configuration includes 200 DTs, a maximum depth of 10, 2 minimum samples per split, 1 minimum samples per leaf, log2 for maximum features, Gini entropy as splitting criterion, and bootstrap sampling. Finally, the ANN achieved optimal performance with a single hidden layer containing 100 neurons and a maximum of 1000 train iterations.

4.2 Models performance

The models’ accuracy metric in the detection of injury-related running patterns depends on the input sets and the specific injury. Table 1 shows the accuracy provided by the evaluated models for all approaches. DL algorithms achieve the highest accuracy across all conditions. The best results are obtained with CNNs, which reach 77.9% accuracy for PFPS when using time series and point values, 73.8% for ITBS with time series, and 71.4% for the combined injury category (PFPS+ITBS) under the same input type. Among machine learning (ML) methods, SVM_L and GP provide the highest accuracy for most condition, making them the most competitive classical models. GP is consistently high across all input data combinations for injury pattern identification, achieving the highest accuracy for PFPS+ITBS with all the input data (63.7% accuracy with time series, 66.1% with time series and point values, and 62.5% with point values). It is particularly effective when using point values, reaching 62.8% in PFPS+ITBS, 69.5% for PFPS, and 62.5% for ITBS. Similarly, SVM_L demonstrates robust performance, with some of the highest in the time series and point values combination: 63.4% accuracy in PFPS+ITBS detection, 71.7% for PFPS, and 60.5% for ITBS. Given these patterns, the following discussion focuses on GP and SVM_L for their superiority among ML methods, and on CNN as the leading DL approach.

The adequacy of input data is highly dependent on the algorithm, even when focusing on GP, SVM_L, and CNN. For PFPS detection, accuracy slightly improves when combining time series and point values: from 71.5% to 71.7% with SVM_L and from 76.2% to 77.9% with the CNN. For PFPS+ITBS, GP increases from 63.7% to 66.0%, and SVM_L shows a similar trend (from 62.2% to 63.4%), whereas the CNN slightly worsens (from 71.4% to 70.5%). In contrast, for ITBS pattern identification, using either point values or time series alone yields the best results. GP provides 63.5% accuracy with time series and 62.5% accuracy with point values, while the combination of both reduces performance to 60.1% accuracy. The highest accuracy for ITBS (73.8%) is also obtained with time series when using the CNN.

Table 2: Precision, recall and F1-score classification metrics of the most accurate methods in injury pattern identification.

Model	Time series			Time series & Point values			Point values			
	PFPS+ITBS	PFPS	ITBS	PFPS+ITBS	PFPS	ITBS	PFPS+ITBS	PFPS	ITBS	
PRE(%)	SVM _L	61.9 \pm 3.9	69.9 \pm 6.3	62.4 \pm 7.8	63.2 \pm 2.2	70.4 \pm 2.1	60.3 \pm 6.2	57.3 \pm 5.3	66.8 \pm 4.9	56.5 \pm 8.9
	GP	64.4 \pm 4.9	61.3 \pm 14.8	62.3 \pm 9.2	66.5 \pm 2.3	64.6 \pm 9.3	59.3 \pm 3.4	62.8 \pm 4.0	68.4 \pm 5.1	63.8 \pm 5.3
	CNN	52.9 \pm 3.5	42.2 \pm 2.5	40.4 \pm 4.9	52.2 \pm 1.4	41.3 \pm 3.0	34.3 \pm 3.0	—	—	—
	LSTM	43.8 \pm 1.0	37.4 \pm 2.2	26.8 \pm 2.7	—	—	—	—	—	—
REC(%)	SVM _L	66.5 \pm 7.2	76.4 \pm 9.5	55.3 \pm 16.8	66.5 \pm 6.9	77.0 \pm 2.5	61.3 \pm 18.8	59.3 \pm 16.5	69.1 \pm 8.9	50.2 \pm 27.7
	GP	63.1 \pm 3.7	80.5 \pm 16.2	60.7 \pm 19.9	65.9 \pm 2.4	78.6 \pm 11.4	59.9 \pm 17.1	63.0 \pm 8.1	73.1 \pm 5.4	60.0 \pm 6.9
	CNN	82.2 \pm 6.6	82.7 \pm 8.1	72.5 \pm 10.2	79.7 \pm 7.3	90.3 \pm 5.8	81.87 \pm 4.6	—	—	—
	LSTM	94.4 \pm 3.6	77.8 \pm 8.1	87.5 \pm 6.6	—	—	—	—	—	—
F1(%)	SVM _L	63.8 \pm 3.6	72.4 \pm 4.7	57.2 \pm 10.8	64.6 \pm 3.0	73.5 \pm 1.4	59.4 \pm 11.3	57.4 \pm 9.8	67.8 \pm 6.3	49.0 \pm 16.1
	GP	63.7 \pm 4.0	66.6 \pm 6.0	60.7 \pm 14.7	66.2 \pm 2.1	69.5 \pm 3.9	58.6 \pm 10.1	62.8 \pm 5.9	70.5 \pm 4.1	61.4 \pm 3.9
	CNN	64.1 \pm 1.7	55.7 \pm 1.4	51.2 \pm 3.0	62.9 \pm 2.1	56.5 \pm 2.1	48.2 \pm 1.6	—	—	—
	LSTM	59.8 \pm 1.2	50.3 \pm 1.7	40.8 \pm 2.6	—	—	—	—	—	—

Table 2 shows the precision, recall and F1-score metrics for the most accurate models-GP, SVM_L and CNN-for a more detailed analysis. GP stands out when using point values, outperforming SVM_L in all metrics, with improvements ranging from 2% to 5% for PFPS+ITBS or PFPS, and up to 11% improvement of the F1-score for ITBS. However, when handling time series or the combination of time series and point values, SVM_L achieves higher precision and F1-score, while GP maintains superior recall. Although both models show similar values for precision, recall, and F1-score, GP is noteworthy for its consistently higher recall, which is particularly relevant as it may better identify true injury patterns. In the case of CNN, additional observations emerge: its precision is relatively low due to the prioritization of recall, meaning that although overall accuracy is high, its F1-score still has room for improvement.

These results suggest that DNNs capture complex differences in motion capture time series data of injury running patterns compared to non-injured patterns, but it is optimized for maximum recall and precision can be improved. The improvement in results when analyzing time series compared to point values supports the claim that time series contain relevant movement information for identifying patterns associated with runner injuries Phinyomark et al. [2017]. SVM_L also handles both time series and point data effectively to identify injury running patterns, and GP is more suitable for using point values.

Compared with our previous study in Fuentes-Jiménez et al. [2025], the reported metrics generally decrease. Although both studies use the same database, the current work applies a stricter data splitting strategy: users are completely separated between the test and training subsets. Unlike the previous approach, when evaluating models in this study, the test data contains no samples from volunteers included in the training data. This distinction makes the present analysis more rigorous and provides results that better reflect a realistic scenario in which the classifier is applied to detect injury patterns in runners who are unknown for the classifier.

4.3 Injury pattern detection

The injury pattern associated to PFPS is detected with the highest overall accuracy. When combining time series and point values, SVM_L, and ANN achieve accuracies above 70% for PFPS pattern identification (see Table 1), and this performance is improved by CNNs, which reach 77.9% accuracy with the same inputs. PFPS+ITBS is generally the second best detected pattern with all methods, except when using point values alone. For PFPS+ITBS, detection accuracy ranges between 60% and 66% for the majority of ML methods when using time series, while CNNs improve ITBS detection with 73.8% accuracy using time series and 73.3% when combining time series and point values. These results support the hypothesis of the relevance of analyzing complete time series, rather than reducing them to point movement values, to identify injury patterns.

These findings are consistent when analyzing the F1-score, which represents a balance between precision and recall. Among ML algorithms, the highest F1-scores are observed for PFPS, followed by the generic case (PFPS+ITBS), and finally ITBS (see Table 2). However, CNNs exhibit a different pattern: their best F1-score occurs in the PFPS+ITBS case because, for PFPS and ITBS specific injuries, precision is significantly reduced to maximize the detection of injury patterns.

The 77.9% accuracy in detecting PFPS indicates that the differences in the angle time series and movement parameters of injured individuals compared to non-injured volunteers are identified by the CNN. In ITBS, certain differences are also utilized for its identification, but the accuracy (73.8%) has more room for improvement. These results are novel compared to previous studies where injured and non-injured volunteers could not be grouped using unsupervised algorithms Dingenen et al. [2020], Jauhainen et al. [2020], Senevirathna et al. [2023]. Thus, the results of this work suggest that advanced algorithms can identify injury patterns in running using motion analysis systems.

The PFPS pattern is detected more accurately when considered individually rather than combined. It supports that running patterns differences are more closely associated with specific injuries rather than a general injury pattern, as found in previous studies Ceyssens et al. [2019]. Also, the improved detection of the PFPS pattern compared to ITBS suggests that the PFPS pattern deviates the most from the non-injured pattern.

The classification metrics in this study align with the idea that ML methods can successfully identify athletes with high risk of injury. The metrics found in this study for PFPS identification are lower than those provided in Eskofier et al. [2012], where results show perfect accuracy. However, the previous study identifies only six injured volunteers and ensures similar features in the non-injured group. In contrast, our study includes more variability, which can explain the lower values in the classification metrics. Previous studies have reported similar high classification accuracy (from 75% to 83%) when predicting injury risks in other sports, such as baseball or Australian football Hans Van Eetvelde et al. [2021], as well as in clinical gait analysis where ML is promoted to support medical decision making Slijepcevic et al. [2021].

4.4 Explainability

The explainability of the ML algorithms is evaluated using cumulative Shapley values to identify the most important input features and analyze their SHAP contributions. We focus on feature importance in SVM_L , as it consistently provides high performance using both time series and point values as input data, allowing us to assess the significance of all parameters under their optimal condition. The analysis is performed separately for each injury pattern detection, shown in Fig. 2a, Fig. 3a, and Fig. 4a, for PFPS+IBTS, PFPS, and ITBS, respectively.

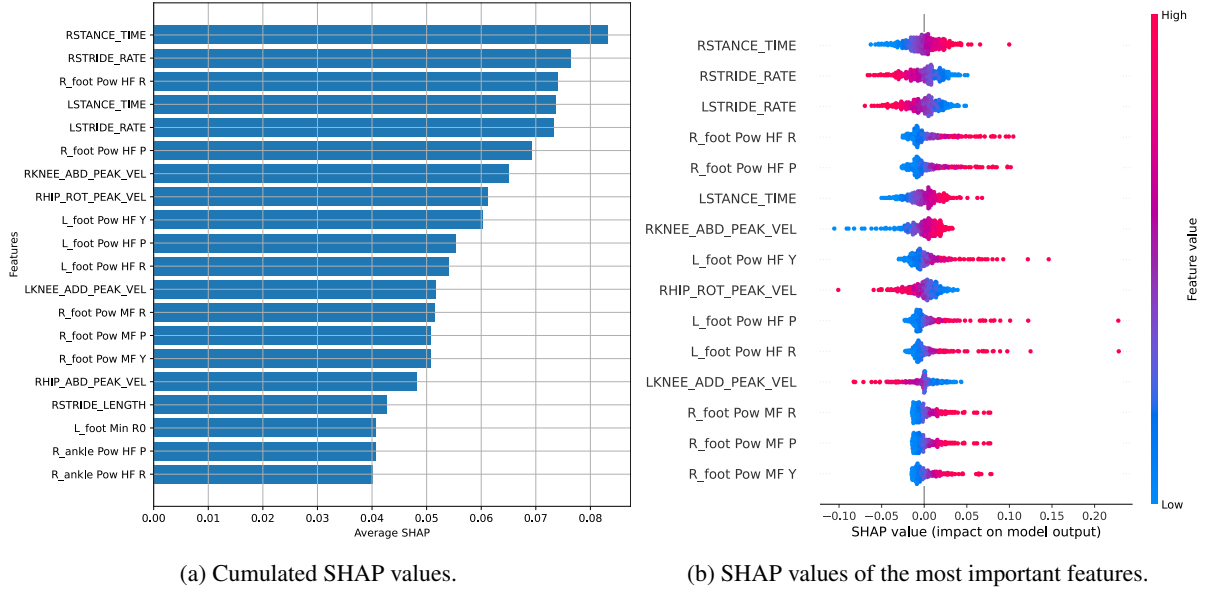


Figure 2: Cumulated normalized SHAP for the most relevant features in the identification of PFPS+ITBS with SVM_L .

We set the boundary to study the most relevant features in the second SHAP value decrement after visual inspection of Fig. 2a, Fig. 3a, and Fig. 4a. This analysis results in analyzing those features with SHAP higher or equal to 0.05 for PFPS+ITBS detection, to 0.03 for PFPS and to 0.35 for ITBS. In this way, we analyze the SHAP value cumulated for the five test sets of 15 features for PFPS+ITBS in Fig. 2b, 11 features for PFPS in Fig. 3b, and also 11 features for ITBS in Fig. 4b.

Analyzing the features with the highest SHAP values, we observe that the relevant features for the generic case, which are in Fig. 2b, generally combine those identified as important for PFPS and ITBS individually (see Fig. 3 and Fig. 4). Examples of relevant features included in both the general and specific injury patterns are the stance time of both feet, which is significant for PFPS and ITBS separately too, the stride rate (relevant for PFPS), and knee abduction peak velocity (relevant for ITBS). Point values, including power in medium and high frequency bands, show greater importance, even though SVM_L achieves better results when the time series data are included, making these temporal feature relevant but not the most decisive when combined with point values. The influence of high or low values of these features, along with the sign of their impact on the model, remains consistent across the generic and individual cases. For instance, a high stance time for both feet is directly associated with injury risk in all three scenarios, PFPS+ITBS,

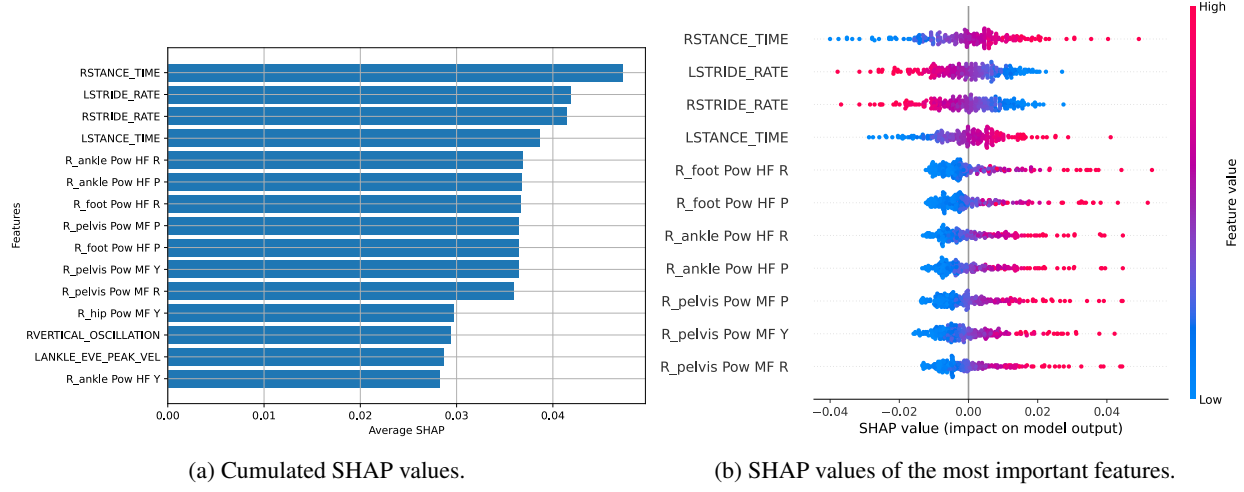


Figure 3: Cumulated normalized SHAP for the most relevant features in the identification of PFPS with SVM_L .

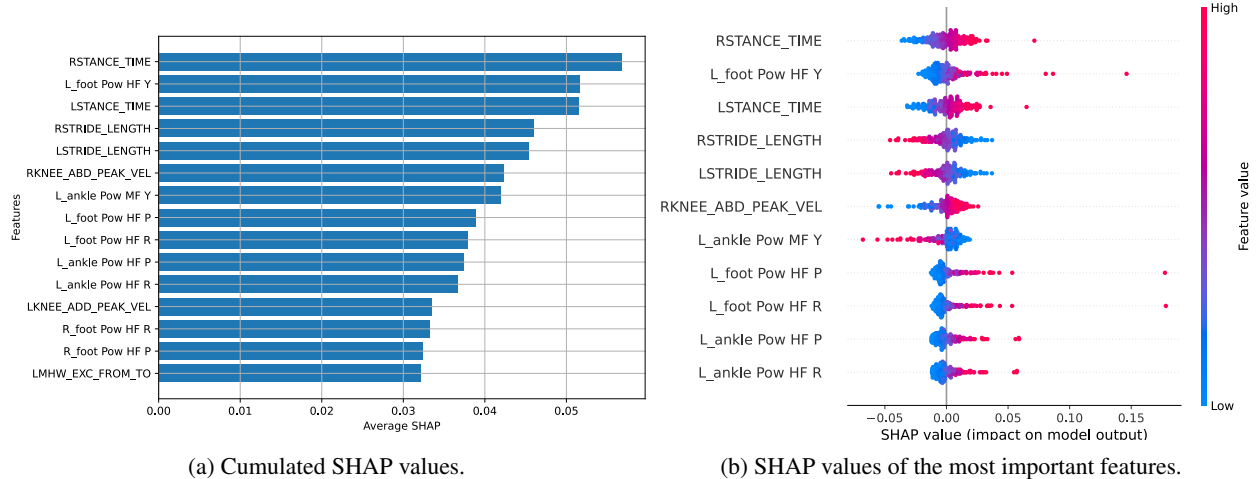


Figure 4: Cumulated normalized SHAP for detection of ITBS with SVM_L .

PFPS, and ITBS identification. This finding indicates that the patterns for PFPS and ITBS differ; however, ML methods enable the analysis of a generic injury pattern in which the parameters most strongly associated with injuries are detected.

The injury patterns for PFPS and ITBS share stance time as a common feature; however, the remaining features—and consequently their overall patterns—differ. The PFPS injury pattern is associated with longer stance time and lower stride rate. It can also be observed that high power in medium and high frequency bands for the foot, ankle, and pelvis is related to this injury risk. ITBS maintains the same direct relationship with stance time, but stride length is also involved, with longer stride lengths being less associated with ITBS injuries. The high and medium frequency components of motion are also relevant for this injury; however, in this case, the most significant joints are the foot and ankle only, excluding the pelvis as in PFPS. Another difference is the relevance of knee abduction peak velocity, where lower values are more strongly associated with reduced ITBS risk.

The explainability maps of the CNN with time series are in Fig. 5 for the generic case, Fig. 6 for PFPS and Fig. 7 for ITBS. For all the injuries, we depict the saliency map, the Grad-CAM and the SHAP values to analyze their consistency. In detecting the three injury patterns—PFPS+ITBS, PFPS and ITBS—there is consistency across the three evaluated maps, as regions with saliency also exhibit elevated Smooth-Grad values and a positive SHAP value of greater magnitude, close to one. For instance, in the generic case in Fig. 5, the time interval between 20% and 40% of the gait cycle consistently appears in red for joints on the left side of the body, which mean they are related with the identification of the injury patterns. Conversely, intervals with less relevance for injury detection, such as the initial phase of the left

side of the body, are in blue in the three maps, showing low salience (Fig. 5a), low Smooth-Grad values (Fig. 5b) and negative SHAP values (Fig. 5c).

There are significant differences between the generic case and the specific cases of PFPS and ITBS. In the generic case, whose explainability is in Fig. 5, the interval with the greatest number of relevant joints for the longest duration occurs during midstance, from the 20% of the stance phase until the 60%. Within this interval, both feet appear as relevant at the beginning or end of this phase of gait. Relevance is also detected at the start and end of the step, although with shorter duration. In PFPS (Fig. 6), two distinguishable relevant areas can be observed, particularly in terms of SHAP values: the beginning of the stance phase (up to 20%) and the point approaching its end (end of midstance). At the start of the step, high relevance is seen in the left ankle and, more notably, in both feet, highlighting the importance of foot placement during initial contact. At the end of midstance, the most relevant joints are the upper ones of the leg, specifically the knee and hip of both legs. Finally, in ITBS, the greatest relevance in Fig. 7 is assigned to the beginning of the stance phase, where the foot and ankle on both sides of the body are important, similar to PFPS. During midstance, relevance shifts to higher joints, such as the hip, similar to the case of PFPS detection.

These explainability maps do not allow for the determination of a clear specific running pattern associated with PFPS or ITBS in our analysis. However, the saliency, Grad-CAM, and Shapley maps enable the identification of the most relevant temporal intervals. As a summary of the patterns specific for this analysis, the generic case (Fig. 5) considers the entire stance phase while varying the relevant joint or segment, covering all of them. In contrast, the intervals most relevant for PFPS (Fig. 6) and ITBS (Fig. 7) are clearly the beginning of the stance phase in the lower part of legs and the end of midstance. This information is valuable for future studies focused on detecting these injury patterns. Additionally, the differences between the generic case, PFPS and ITBS maps, regarding these relevant intervals and the joints that most influence the analysis, clearly show that the running pattern differs between the two evaluated injuries. These insights provide promising results for the establishment of generic and specific running injury patterns.

5 Conclusions

This study evaluates the detection of running patterns associated with PFPS and ITBS applying a supervised ML framework, including classical and DNN methods, in motion capture data. CNNs and LSTMs outperform classical ML models in detecting those running patterns. The PFPS detection (77.9%) demonstrates that CNNs effectively identifies differences in angle time series and movement parameters between injured and non-injured runners. Although ITBS detection (73.8) also indicates certain differences, but less than in PFPS. These findings highlight the potential of research in differentiating injury patterns. The PFPS+ITBS identification analysis (71.4%) also demonstrates promising results to find a generic injury pattern. Additionally, models trained on rotation angle time series consistently outperform those using only kinematic descriptors, highlighting the importance of technologies that analyze the complete motion.

The classification algorithms are assessed in terms of their explainability using Shapley, saliency maps and Grad-CAM, to interpret the models' decisions. In the analysis of classical ML algorithms, there is significant variability in the relevant features for PFPS and ITBS, and the generic scenario consistently find relevant the combination of these specific cases. When analyzing the complete time series relevance in the CNN, the relevant time intervals also differ between PFPS and ITBS injury patterns, proving motion capture systems measure subtle differences between these patterns.

In conclusion, this study supports the use of explainable models in running analysis that analyzes motion kinematics. It provides promising results for future developments of personalized injury prevention tools. Future work may explore other DNN technologies that further exploit more the relationship between features and analyze the effect of feature order and its padding. Furthermore, future studies should aim to extrapolate this analysis to portable sensing technologies, enabling a more representative assessment of running biomechanics in real-world environments.

References

- S Videbaek, AM Bueno, RO Nielsen, and S Rasmussen. Incidence of running-related injuries per 1000 h of running in different types of runners: a systematic review and meta-analysis. *Sports Medicine*, 45(7):1017–1026, 2015.
- JE Taunton, MB Ryan, DB Clement, DC McKenzie, DR Lloyd-Smith, and BD Zumbo. A retrospective case-control analysis of 2002 running injuries. *British Journal of Sports Medicine*, 36(2):95–101, 2002.
- MP Van der Worp, DS ten Haaf, R van Cingel, A de Wijer, MW Nijhuis-van der Sanden, and JB Staal. Injuries in runners; a systematic review on risk factors and sex differences. *PLoS One*, 10(2):e0114937, 2015.
- Harrison Philip Crowell and Irene S Davis. Gait retraining to reduce lower extremity loading in runners. *Clinical biomechanics*, 26(1):78–83, 2011.

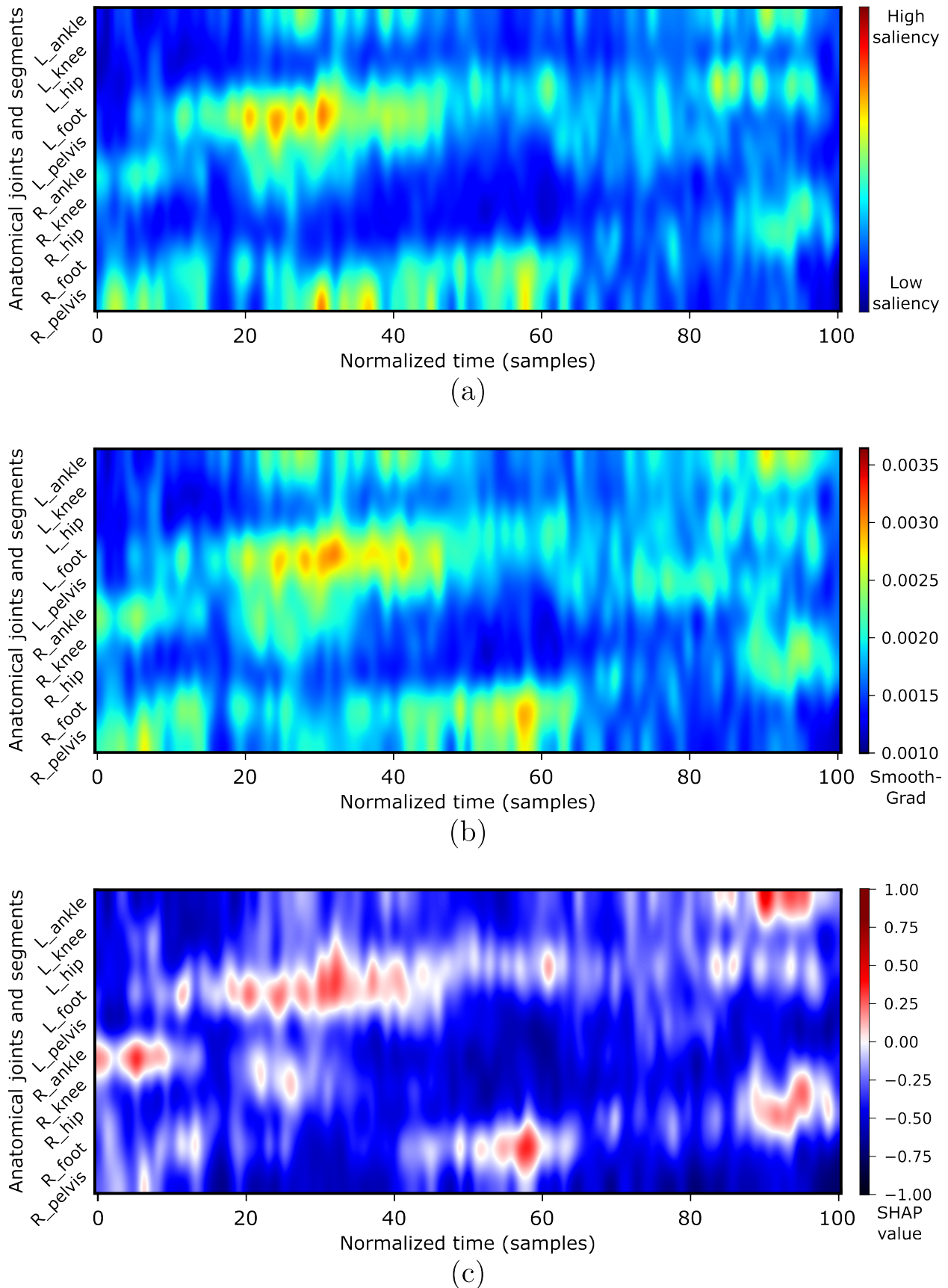


Figure 5: CNN explainability for PFPS+ITBS identification with temporal features from three methods: (a) depicts the saliency map, (b) corresponds to Grad-CAM and (c) is the shapley analysis result.

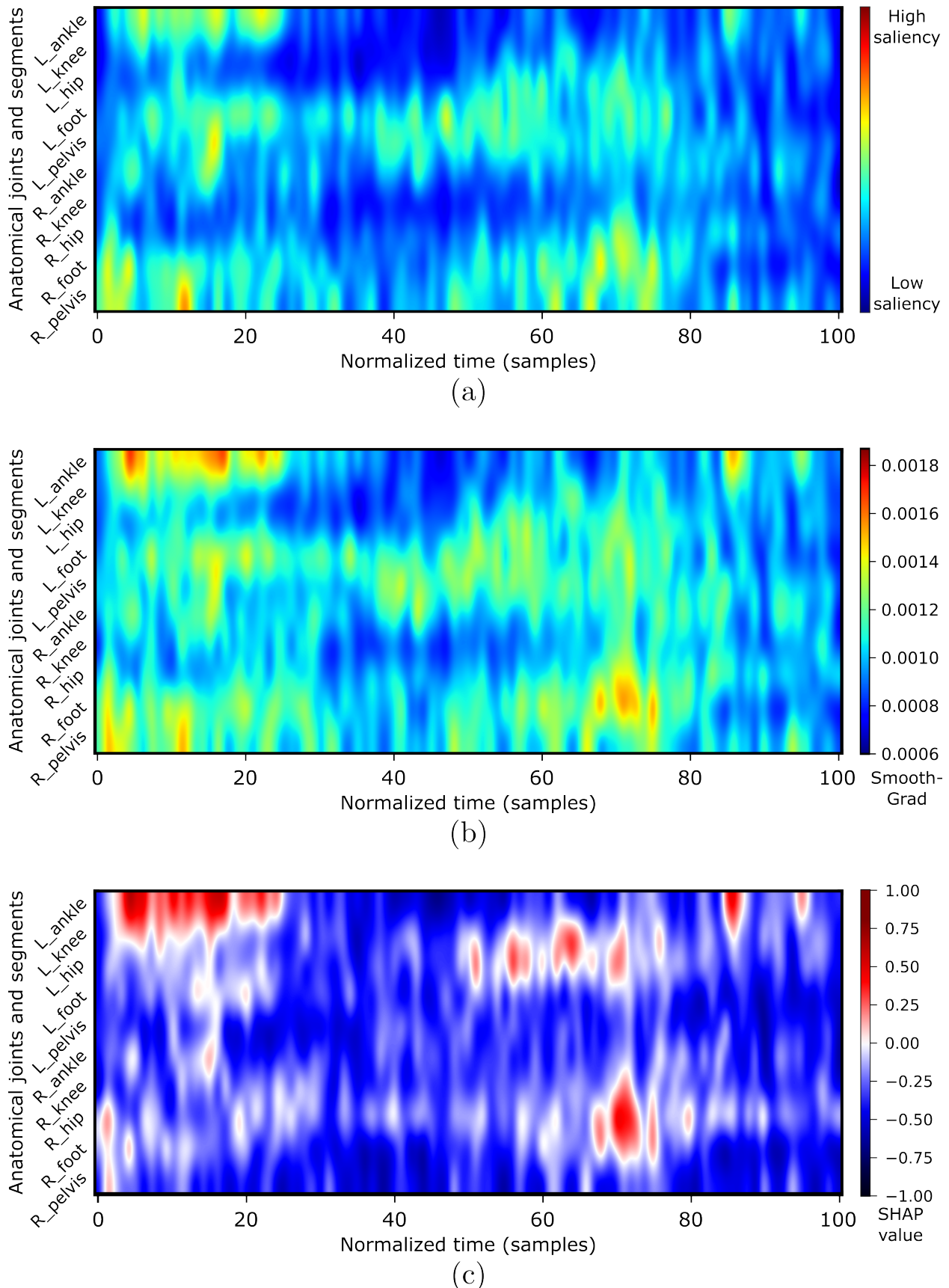


Figure 6: CNN explainability for PFPS identification with temporal features from three methods: (a) depicts the saliency map, (b) corresponds to Grad-CAM and (c) is the shapley analysis result.

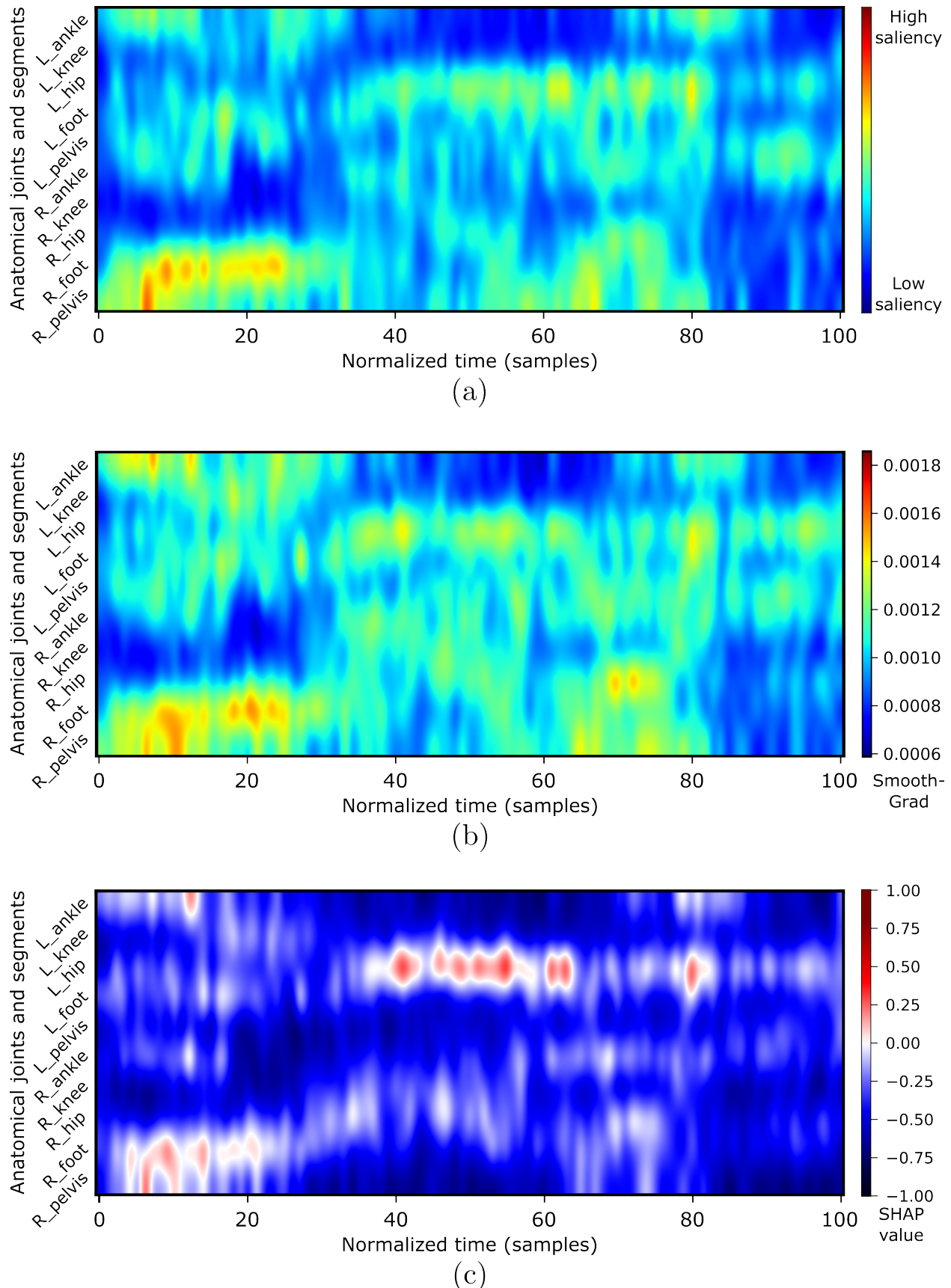


Figure 7: CNN explainability for ITBS identification with temporal features from three methods: (a) depicts the saliency map, (b) corresponds to Grad-CAM and (c) is the shapley analysis result.

Saghar Soltanabadi, Hooman Minoonejad, Mohammad Bayattork, and Mohammad Seyedahmadi. Effect of virtual reality and augmented reality training for injury prevention and accelerating rehabilitation of anterior cruciate ligament injury in athletes: A scoping review. *Asian Journal of Sports Medicine*, 14(4), 2023.

Meghan Keast, Jason Bonacci, and Aaron Fox. Acute effects of gait interventions on tibial loads during running: A systematic review and meta-analysis. *Sports Medicine*, 52(10):2483–2509, 2022.

Grazia Cicirelli, Donato Impedovo, Vincenzo Dentamaro, Roberto Marani, Giuseppe Pirlo, and Tiziana R D’Orazio. Human gait analysis in neurodegenerative diseases: A review. *IEEE journal of biomedical and health informatics*, 26(1):229–242, 2021a.

Mohammed Hammoud, Aleksei Shcherbak, Olga Istrakova, Nataliya Shindryaeva, Ekaterina Bril, Roberto Passerone, and Andrey Somov. Wrist-worn sensors and machine learning for parkinson’s disease detection: Investigation of binary and multi-classification problem. *IEEE Transactions on Instrumentation and Measurement*, 2025.

Aleksei Shcherbak, Ekaterina Kovalenko, and Andrey Somov. Detection and classification of early stages of parkinson’s disease through wearable sensors and machine learning. *IEEE Transactions on Instrumentation and Measurement*, 72:1–9, 2023.

Hoonyong Lee, Gaang Lee, SangHyun Lee, and Changbum R Ahn. Assessing exposure to slip, trip, and fall hazards based on abnormal gait patterns predicted from confidence interval estimation. *Automation in Construction*, 139:104253, 2022.

Wei Zeng, Shiek Abdullah Ismail, and Evangelos Pappas. Detecting the presence of anterior cruciate ligament injury based on gait dynamics disparity and neural networks. *Artificial Intelligence Review*, 53(5):3153–3176, 2020.

Christos Kokkotis, Serafeim Moustakidis, Themistoklis Tsatalas, Charis Ntakolia, Georgios Chalatsis, Stylianos Konstadakos, Michael E Hantes, Giannis Giakas, and Dimitrios Tsaopoulos. Leveraging explainable machine learning to identify gait biomechanical parameters associated with anterior cruciate ligament injury. *Scientific Reports*, 12(1):6647, 2022.

Yifang Zhuang, Wenxing Zhou, Ziwei Zeng, Shiwei Mo, and Lin Wang. Influences of footstrike patterns and overground conditions on lower extremity kinematics and kinetics during running: Statistical parametric mapping analysis. *PLOS ONE*, 20(2):e0317853, February 2025. ISSN 1932-6203. doi:10.1371/journal.pone.0317853. URL <http://dx.doi.org/10.1371/journal.pone.0317853>.

Linde Ceyssens, Romy Vanelderen, Christian J Barton, Peter Malliaras, and Bart Dingenen. Biomechanical risk factors associated with running-related injuries: a systematic review. *Sports Medicine*, 49(7):1095–1115, 2019.

Angkoon Phinyomark, Giovanni Petri, Esther Ibáñez-Marcelo, Sean T. Osis, and Reed Ferber. Analysis of big data in gait biomechanics: Current trends and future directions. *Journal of Medical and Biological Engineering*, 38(2):244–260, July 2017. ISSN 2199-4757. doi:10.1007/s40846-017-0297-2. URL <http://dx.doi.org/10.1007/s40846-017-0297-2>.

Steffen Willwacher, Markus Kurz, Johanna Robbin, Matthias Thelen, Joseph Hamill, Luke Kelly, and Patrick Mai. Running-related biomechanical risk factors for overuse injuries in distance runners: A systematic review considering injury specificity and the potentials for future research. *Sports Medicine*, 52(8):1863–1877, March 2022. ISSN 1179-2035. doi:10.1007/s40279-022-01666-3. URL <http://dx.doi.org/10.1007/s40279-022-01666-3>.

Bart Dingenen, Filip Staes, Romy Vanelderen, Linde Ceyssens, Peter Malliaras, Christian J Barton, and Kevin Deschamps. Subclassification of recreational runners with a running-related injury based on running kinematics evaluated with marker-based twodimensional video analysis. *Physical Therapy in Sport*, 44:99–106, 2020.

Susanne Jauhainen, Andrew J Pohl, Sami Äyrämö, Jukka-Pekka Kauppi, and Reed Ferber. A hierarchical cluster analysis to determine whether injured runners exhibit similar kinematic gait patterns. *Scandinavian Journal of Medicine and Science in Sports*, 30:732–740, 2020.

Jack A Martin, Stiffler-Joachim. Mikel R, and Bryan C Wille, Christa Mand Heiderscheit. A hierarchical clustering approach for examining potential risk factors for bone stress injury in runners. *Journal of Biomechanics*, 141:111136, 2022.

Angela M Senevirathna, Andrew J Pohl, Matthew Jordan, William Brent Edwards, and Reed Ferber. Differences in kinetic variables between injured and uninjured rearfoot runners: A hierarchical cluster analysis. *Scandinavian Journal of Medicine and Science in Sports*, 33:160–168, 2023.

Bjoern M Eskofier, Martin Kraus, Jay T Worobets, Darren J Stefanyskyn, and Benno M Nigg. Pattern classification of kinematic and kinetic running data to distinguish gender, shod/barefoot and injury groups with feature ranking. *Computer Methods in Biomechanics and Biomedical Engineering*, 15(5):467–474, 2012.

David Fuentes-Jiménez, Sara García-de Villa, David Casillas-Pérez, Pablo Floría, and Francisco-Manuel Melgarejo-Meseguer. Advanced machine learning techniques for explainable detection of knee injuries in runners. In *2025 IEEE Medical Measurements & Applications (MeMeA)*, pages 1–6, 2025. doi:10.1109/MeMeA65319.2025.11068035.

Grazia Cicirelli, Donato Impedovo, Vincenzo Dentamaro, Roberto Marani, Giuseppe Pirlo, and Tiziana R D’Orazio. Human gait analysis in neurodegenerative diseases: A review. *IEEE journal of biomedical and health informatics*, 26(1):229–242, 2021b.

Yi Xia and Aisheng Cao. Multimodal dynamic-static combined graph convolutional network for detecting freezing of gait. *Biomedical Signal Processing and Control*, 112:108368, 2026.

M Ramkumar Raja, G Hari Krishnan, Amanulla Mohammad, and Sreevardhan Cheerla. Dual temporal gated multi-graph convolution network based neurodegenerative disease detection and severity prediction. *Biomedical Signal Processing and Control*, 112:108566, 2026.

Yi Ru, Xiangwei Zhao, Yasamin Baghersad, Hamid Taheri Andani, Maboud Hekmatifar, and Belgacem Bouallegue. Gait analysis and machine learning algorithms to distinguish between parkinson’s disease, amyotrophic lateral sclerosis, and huntington’s disease. *Biomedical Signal Processing and Control*, 110:108216, 2025.

Felipe Arruda Moura, Alexandre RM Pelegrinelli, Danilo S Catelli, Mario Lamontagne, and Ricardo da Silva Torres. Knee osteoarthritis prediction from gait kinematics: Exploring the potential of deep neural networks and transfer learning methods for time series classification. *Journal of Biomechanics*, page 112881, 2025.

Sara García-de-Villa, Luisa Ruiz-Ruiz, Guillermo García-Villamil-Neira, Marta Álvarez Neira, Elisabet Huertas-Hoyas, Antonio J Del-Ama, M Crtistina Rodriguez-Sánchez, Fernando Seco, and Antonio R Jiménez. Validation of an imu-based gait analysis method for assessment of fall risk against traditional methods. *IEEE journal of biomedical and health informatics*, 2024.

Yuchao Liu, Jiajie Guo, Chuxuan Guo, Zijie Liu, Yiran Tong, Xuan Wu, Qining Wang, and Caihua Xiong. Muscle-joint feature fusion for swimming pattern recognition with 1d- cnn classifier. *IEEE Transactions on Instrumentation and Measurement*, 2025.

Weizheng Chen and Yue Jia. Kinetic chain analysis of tennis stroke motion utilizing wearable sensors. *IEEE Transactions on Instrumentation and Measurement*, 2025.

Reed Ferber, Allan Brett, Reginaldo K Fukuchi, Blayne Hettinga, and Sean T Osis. A biomechanical dataset of 1,798 healthy and injured subjects during treadmill walking and running. *Scientific Data*, 11(1):1232, 2024.

Sean T Osis, Blayne A Hettinga, Jessica Leitch, and Reed Ferber. Predicting timing of foot strike during running, independent of striking technique, using principal component analysis of joint angles. *Journal of biomechanics*, 47(11):2786–2789, 2014.

Gregory Shakhnarovich, Trevor Darrell, and Piotr Indyk. Nearest-neighbor methods in learning and vision. *IEEE Transactions on Neural Networks*, 19(2):377, 2008.

Gareth James, Daniela Witten, Trevor Hastie, and Robert Tibshirani. *An Introduction to Statistical Learning*. Springer New York, 2013. ISBN 9781461471387. doi:10.1007/978-1-4614-7138-7. URL <http://dx.doi.org/10.1007/978-1-4614-7138-7>.

Bernhard Schölkopf, Alexander J Smola, Francis Bach, et al. *Learning with kernels: support vector machines, regularization, optimization, and beyond*. MIT press, 2002.

Carl Edward Rasmussen. Gaussian processes in machine learning. In *Summer school on machine learning*, pages 63–71. Springer, 2003.

Lior Rokach and Oded Maimon. Decision trees. In *Data mining and knowledge discovery handbook*, pages 165–192. Springer, 2005.

Artur J Ferreira and Mário AT Figueiredo. Boosting algorithms: A review of methods, theory, and applications. *Ensemble Machine Learning*, pages 35–85, 2012.

Sergio González, Salvador García, Javier Del Ser, Lior Rokach, and Francisco Herrera. A practical tutorial on bagging and boosting based ensembles for machine learning: Algorithms, software tools, performance study, practical perspectives and opportunities. *Information Fusion*, 64:205–237, 2020.

Leo Breiman. Random forests. *Machine Learning*, 45(1):5–32, 2001.

Christopher M Bishop et al. *Neural networks for pattern recognition*. Oxford university press, 1995.

Yann LeCun, Yoshua Bengio, and Geoffrey Hinton. Deep learning. *nature*, 521(7553):436–444, 2015.

Christian Szegedy, Sergey Ioffe, Vincent Vanhoucke, and Alexander A. Alemi. Inception-v4, inception-resnet and the impact of residual connections on learning. In *Proceedings of the Thirty-First AAAI Conference on Artificial Intelligence*, AAAI'17, page 4278–4284. AAAI Press, 2017.

Jie Hu, Li Shen, and Gang Sun. Squeeze-and-excitation networks. In *2018 IEEE/CVF Conference on Computer Vision and Pattern Recognition*, pages 7132–7141, 2018. doi:10.1109/CVPR.2018.00745.

Sepp Hochreiter and Jürgen Schmidhuber. Long short-term memory. *Neural Computation*, 9(8):1735–1780, November 1997. ISSN 1530-888X. doi:10.1162/neco.1997.9.8.1735. URL <http://dx.doi.org/10.1162/neco.1997.9.8.1735>.

Erik Štrumbelj and Igor Kononenko. Explaining prediction models and individual predictions with feature contributions. *Knowledge and Information Systems*, 41(3):647–665, August 2013. ISSN 0219-3116. doi:10.1007/s10115-013-0679-x. URL <http://dx.doi.org/10.1007/s10115-013-0679-x>.

Karen Simonyan, Andrea Vedaldi, and Andrew Zisserman. Deep inside convolutional networks: Visualising image classification models and saliency maps. *arXiv preprint arXiv:1312.6034*, 2013.

Ramprasaath R. Selvaraju, Michael Cogswell, Abhishek Das, Ramakrishna Vedantam, Devi Parikh, and Dhruv Batra. Grad-cam: Visual explanations from deep networks via gradient-based localization. In *2017 IEEE International Conference on Computer Vision (ICCV)*, page 618–626. IEEE, October 2017. doi:10.1109/iccv.2017.74. URL <http://dx.doi.org/10.1109/ICCV.2017.74>.

Hans Van Eetvelde, Luciana D. Mendonça, Christophe Ley, Romain Seil, and Thomas Tischer. Machine learning methods in sport injury prediction and prevention: a systematic review. *Journal of Experimental Orthopaedics*, 8(27), 2021.

Djordje Slijepcevic, Fabian Horst, Sebastian Lapuschkin, Brian Horsak, Anna-Maria Raberger, Andreas Kranzl, Wojciech Samek, Christian Breiteneder, Wolfgang Immanuel Schöllhorn, and Matthias Zeppelzauer. Explaining machine learning models for clinical gait analysis. *ACM Transactions on Computing for Healthcare*, 3(2), 2021. doi:10.1145/3474121. URL <https://doi.org/10.1145/3474121>.